Microelectronic Engineering 93 (2012) 91–94

Contents lists available at SciVerse ScienceDirect

Microelectronic Engineering

journal homepage: www.elsevier.com/locate/mee

Study of surface morphology and refractive index of dielectric and metallic films used for the fabrication of monolithically integrated surface plasmon resonance biosensing devices

Alvaro Jimenez, Dominic Lepage, Jacques Beauvais, Jan J. Dubowski *

Department of Electrical and Computer Engineering, Interdisciplinary Institute for Technological Innovations (3IT), Université de Sherbrooke, Sherbrooke, Québec, Canada J1K 2R1

ARTICLE INFO

Article history:
Received 19 April 2011
Received in revised form 23 September 2011
Accepted 20 October 2011
Available online 19 November 2011

Keywords:
Gold thin films
Dielectric thin films
Surface plasmon resonance integrated device
Plasmonic device fabrication
Biosensing

ABSTRACT

Integration in a single chip using localized optical phenomena is one of the possible approaches to attain the accuracy, portability and affordability required for future biosensing devices. We address this problem by investigating a grating-coupled quantum well (QW) surface plasmon resonance (SPR) device that comprises a monolithically integrated source of light and a bio-sensitive surface. The successful operation of such a device requires, in addition to the optimization of its architecture, the use of high quality thin films with smooth surface morphology. Here, we present the results of studying a variety of dielectric and Au films intended for the fabrication of QW-SPR devices. For dielectrics, we found that SiO_2 films obtained by plasma-enhanced chemical vapor deposition have the best surface morphology and optical properties appropriate for our device. The films of Au fabricated with deposition rates exceeding 0.3 nm/s exhibited relatively smooth surface morphology, however the presence of surface micro-inclusions reduced the attractiveness of such films. To avoid sample overheating that occurs at extremely slow deposition rates, we optimized the fabrication of Au films at 0.05 and 0.2 nm/s.

1. Introduction

The surface plasmon resonance (SPR) phenomenon has created numerous opportunities for biosensing primarily related to the shortened time to detection and increased yield of biological tests without the need of dedicated markers [1,2]. Nonetheless, the spread of commercial SPR equipment has been limited to specific research applications, in part due to the elevated cost of the equipment [3]. Consequently, researchers are examining alternative strategies for SPR biosensing that would involve innovative instrumentation allowing a reduced cost of ownership without significantly decreasing the sensitivity and selectivity of the SPR device [1,3].

Conventionally, the development of integrated SPR systems was limited to the fabrication of systems where the optical elements (source and detector) were inherently separated from each other. The use of industrial processes for the manufacture of semiconductor emitters and VLSI microelectronic appliances has open the possibility of studying fabrication processes capable of delivering devices with monolithically integrated optical components, such as light sources and photo detectors. In a previous study [4,5], we demonstrated that an integrated device consisting of a GaAs-$Al_XGa_{1-X}As$ quantum well (QW) microstructure and a dielectric layer covered by a thin metallic film could couple surface plasmon (SP) waves at the metal surface used for analysis. Such SP waves could be scattered through a surface grating and measured in the optical far field. The technique of hyperspectral imaging has recently been used to detect the variations of SP waves at the surface of a QW-SPR micro-device [6].

It is well known that the roughness of SP-coupling metallic films has an impact on the quality factor and coupling efficiency of the SPR effect [7–11]. To address this issue, we report the results of a study focused on the optimization of deposition processes employed for the fabrication of dielectric and Au films that were used to fabricate an optimized QW-SPR device.

2. Sample fabrication

A schematic idea of our monolithically integrated SPR device is illustrated in Fig. 1. It consists of a nominally undoped GaAs/AlGaAs multilayer structure (V0729) grown by molecular beam epitaxy on a semi-insulating (001) GaAs substrate. The multilayer structure is comprised of a $20 \times$ (2.4 nm GaAs/2.4 nm AlGaAs) superlattice grown on a 100 nm buffer layer of GaAs. This was followed by a 300 nm thick layer of GaAs and a set of 3 and 5.5 nm thick GaAs QWs overlaid with 50, 90 and 25 nm $Al_{0.33}Ga_{0.67}As$ barriers. The microstructure was capped with a 5 nm thick GaAs layer

* Corresponding author.
E-mail address: jan.j.dubowski@usherbrooke.ca (J.J. Dubowski).
URL: http://www.dubowski.ca (J.J. Dubowski).

0167-9317/$ - see front matter © 2011 Elsevier B.V. All rights reserved.
doi:10.1016/j.mee.2011.10.016

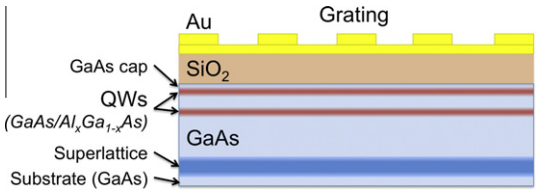

Fig. 1. Schematics of an integrated QW-SPR microstructure designed for biosensing applications. No intermediated layer was applied that normally is used to increase the adhesion of the metallic Au film to the surface of SiO_2.

followed by a 472 nm thick SiO_2 dielectric layer and a 20 nm thick layer of Au. At room temperature, the multilayer structure emits a photoluminescence peak at 870 nm. The extraction of SP waves for detection is achieved with a grating structure fabricated on top of the device. A 750 nm period (P) Au grating with 20 nm high ridges and a ridge to groove ratio of 0.4 is built on top of the Au layer. It is important to clarify that no intermediate layer is employed to enhance the gold-dielectric adhesion, as additional metals would interfere with the studied SPR phenomena. This creates a fabrication challenge because the lift-off process has to be carried out as the last step, and the weak adhesion of Au could result in a compromised quality of the device. We applied the standard e-beam lithography process for the fabrication of these samples.

The study of dielectric materials included thin films of SiO_2, Si_3N_4 and polymethyl methacrylate (PMMA) resist. We used plasma-enhanced chemical vapor deposition (PECVD) [STS model MESC multiplex CVD] for deposition of SiO_2 and Si_3N_4, plasma sputtering [Plasmionique model SPT 320] and e-beam evaporation [BOC Edwards model Auto 306] for SiO_2 and spin coating for deposition of PMMA [Laurell model WS-400-6NPP/Lite/Ind]. We investigated Au films deposited with the BOC Edwards system at 10 different rates (0.01, 0.02, 0.05, 0.07, 0.1, 0.15, 0.2, 0.3, 0.5 and 0.7 nm/s). In all cases, the Au films were 20 nm thick. The samples were characterized using an atomic force microscope (AFM) [Digital Instruments Scanning Probe Microscope], an ellipsometer [J.A. Woollam Co. Inc. model Alpha-SE] and a scanning electron microscope (SEM) [Zeiss model Supra 55VP]. Based on the ellipsometry data, the optical constants were calculated using the B-Spline and the Cauchy models for the metal and dielectric films, respectively [12], fitted with a 0.1% of uncertainty [13].

The surface quality was examined for sampling areas changing from 1 μm × 1 μm to 100 μm × 100 μm. To test the impact of the roughness on the optical response of the material, we employed ellipsometry measurements carried out for sampling areas of approximately 1 mm × 1 mm.

The SPR response from the QW-SPR samples was monitored using a hyperspectral SPR imaging technique. This approach allowed tracking different diffraction angles and energies emitted from the integrated optical device. More details concerning these measurements can be found elsewhere [6].

3. Results and discussion

Fig. 2a shows the results of the surface roughness measured for dielectric films deposited with different techniques. The wavelength dependence of the real part of the refraction index n obtained for 400, 450 and 150 nm thick SiO_2, Si_3N_4 and PMMA samples is shown in Fig. 2b. The extinction coefficient, i.e., the imaginary part of the refractive index k, is near zero for the presented wavelengths. It can be seen that SiO_2 films fabricated by the PECVD technique are characterized by the smoothest surface (R_{ellip} = 1.2 nm). They are also characterized by the relatively small refractive indices as, e.g., n = 1.467 at 870 nm. The e-beam evaporated SiO_2 films were characterized by slightly smaller refractive indices, but their relatively rough surface ($R_{ellip} \approx 4$ nm) discriminate them from the successful application. Clearly, the films with smooth surface morphology and small k values are required to improve the S/N ratio in the detection of the SP waves diffracted by SPR microstructures. The ellipsometry results were complemented by the AFM measurements (see Supplementary data).

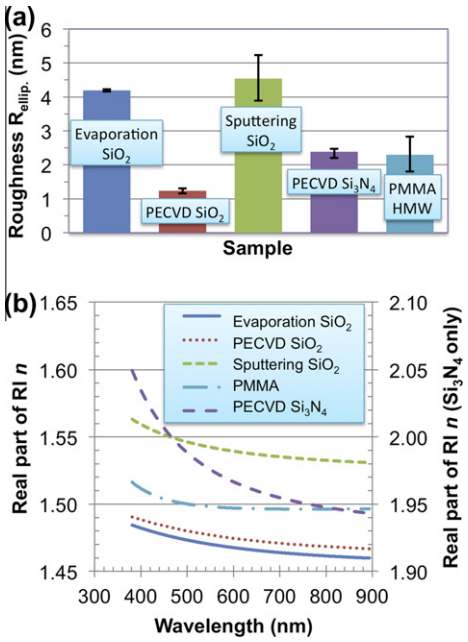

Fig. 2. Roughness of the ellipsometry measured surface (R_{ellip}) of dielectric materials (a), and optical constant (n) of films obtained by evaporation (SiO_2), PECVD (SiO_2 and Si_3N_4), plasma sputtering (SiO_2) and spin coating of resist (PMMA) deposition techniques (b).

Fig. 3a shows the dependence of surface roughness of Au films on the rate of deposition obtained from ellipsometry (R_{ellip}) and AFM (R_{AFM}) measurements. For samples analyzed with the ellipsometry technique, the measurements were repeated in three different regions, resulting in the error amplitudes indicated by the vertical bars in this figure. The decrease of the roughness amplitude is demonstrated with both techniques, primarily in the range of deposition rate increasing from 0.07 to 0.15 nm/s. A somewhat smaller range of changing R_{ellip}, from 1.25 to 0.9 nm, in comparison to R_{AFM}, from 2.3 to 0.8 nm, is likely related to the averaging effect inherent to the data analysis provided by the ellipsometry technique. The results concern the same films thickness, thus, the increased roughness of the low-deposition rate films could be related to the increased time required for their completion. This is illustrated in Fig. 3b where we compare SEM micrographs of films deposited at 0.07 and 0.7 nm/s, i.e., completed within 286 and 28.6 s, respectively. For the low-deposition rate films, the presence of grains and clusters being relatively larger than those present in the fast-rate deposited films can clearly be seen. This observation is in agreement with the results reported in the literature [7,14,15]. The smooth surface of films deposited at rates exceeding 0.2 nm/s would be desirable for the fabrication of QW-SPR integrated devices. However, we observed an excessive amount of micro-inclusions in such films. In Fig. 3c we provide examples of AFM pictures that illustrate this problem. The presence of micro-inclusions (black dots with elevated height over the average level of the surface) is clearly observed on the surface of a 0.7 nm/s deposited film. Micro-clusters of the material e-beam ejected from the Au target at higher deposition rates are likely the source of these micro-inclusions. In contrast, the material deposited at 0.07 nm/s is practically free of these surface defects.

Fig. 3d shows the dependence of the real (n) and imaginary parts (extinction coefficient, k) of the refractive index as a function

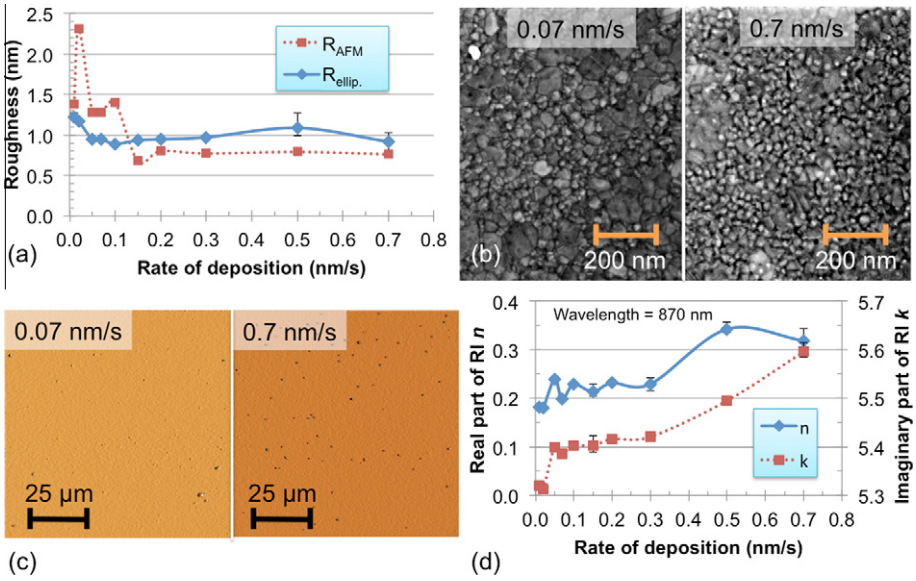

Fig. 3. Roughness of Au films determined by the ellipsometry (R_{ellip}) and AFM (R_{AFM}) measurements for different rates of deposition (a), SEM images of the surface for samples deposited at 0.07 and 0.7 nm/s (b), AFM images of samples obtained for the same evaporation rates (c), and the real (n) and imaginary (k) parts of the refraction index at 870 nm (d).

of the Au films deposition rate. The results are reported for $\lambda = 870$ nm. Significant increase of n and k is observed for the films deposited at rates exceeding 0.3 nm/s. The likely reason for this increase is the presence of surface micro-inclusions observed in Fig. 3c. This suggests that fabrication of technologically attractive Au films, where low surface corrugation is required, should be carried out at deposition rates not exceeding 0.3 nm/s.

As a result of this study, we conclude that optimized SiO_2 films were to be deposited by PECVD, while Au films e-beam evaporated at 0.15 nm/s represent the most desirable materials for the construction of a QW-SPR device. However, we made the fabrication of our sample using deposition rates of Au at 0.5 nm/s for the base layer and 0.02 nm/s for the grating. This enabled us to investigate the quality of the SPR signal for the region where the tradeoff between roughness and optical constants has the best values. The choice of a relatively fast deposition rate of Au films is additionally dictated by the necessity to avoid excessive exposure of samples to the high temperature environment of the e-beam evaporator that was found responsible for the reduced quality of the subsequent lift-off process.

Fig. 4 shows SEM pictures of a QW-SPR device cross-section (Fig. 4a) and an angled view (Fig. 4b) that reveal the dielectric film and a 750 nm period Au grating. The location of Au and QWs is shown in Fig. 4b with arrows, while the darker zone below the 300 nm thick GaAs indicates a location of the superlattice region. Roughness of the surface seen in Fig. 4b is a result of the convolution of the roughness of SiO_2 ($R_{AFM} = 2.6$ nm) and Au ($R_{AFM} = 1.3$ and 0.8 for 0.05 and 0.2 nm/s deposition rates, respectively) deposited on the GaAs substrate. It is reasonable that the roughness amplitude observed in this case is slightly greater than that observed in Figs. 2 and 3 that report the results for a single Au layer deposited directly on the Si substrate. The SPR response and other technical parameters concerning the functioning of this device have been reported elsewhere [6].

4. Conclusions

We have investigated nanofabrication processes required for the construction of QW-SPR devices designed for biosensing applications. An integrated micro-assembly of the QW-SPR device comprises a QW microstructure covered with a dielectric layer and a metallic nano-scale grating. The optical quality of these materials, in particular the surface morphology of the metallic film, plays a critical role in the ability to extract SP waves scattered in the far-field through the nanograting. Our studies have indicated that the PECVD deposited SiO_2 films have attractive optical properties ($n = 1.467$ at 870 nm and $R_{ellip} = 1.2$ nm) for the investigated microstructures. The Au films fabricated with deposition rates not exceeding 0.3 nm/s are desirable for the production of planar films, free of micro-inclusions appearing at greater deposition rates. However, to avoid overheating of the photoresist, which could take

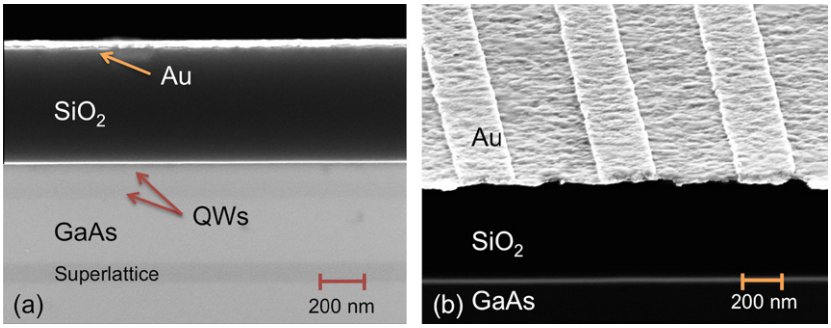

Fig. 4. SEM micrographs of a QW-SPR device cross-section (a) and an angled view (b) that reveal the 472 nm thick dielectric film. The arrows indicate the position of a 20 nm thick Au grating and 2 QWs near the surface. The Au contact layer and the nanograting ridges were deposited at 0.05 and 0.2 nm/s, respectively.

place during extremely slow deposition, the preferred deposition rate of Au films used for nanograting fabrication was chosen between 0.05 and 0.2 nm/s. With the optimized parameters of depositing both SiO_2 and Au films, the high quality QW-SPR devices have been fabricated exhibiting their attractive response for biosensing applications.

Acknowledgments

Funding for this research was provided by the Canada Research Chair in Quantum Semiconductors Program, the Natural Science and Engineering Research Council of Canada (NSERC Strategic Grant STPGP 350501-07) and the Vanier Canada Graduate Scholarship Program. The help of Dr. Khalid Moumanis and all the technical personnel of the Center de recherche en nanofabrication et nanocharacterization (CRN^2) is also acknowledged.

Appendix A. Supplementary data

Supplementary data associated with this article can be found, in the online version, at doi:10.1016/j.mee.2011.10.016.

References

[1] M. Piliarik, J. Homola, SPR Sensor Instrum. 4 (2006) 95–116.
[2] K. Campbell, A.-C. Huet, C. Charlier, C. Higgins, P. Delahaut, C.T. Elliott, J. Chromatogr. B 877 (2009) 4079–4089.
[3] R.L. Caygill, G.E. Blair, P.A. Miller, Anal. Chim. Acta 681 (2010) 8–15.
[4] D. Lepage, J.J. Dubowski, Appl. Phys. Lett. 91 (2007) 163106-1–163106-3.
[5] D. Lepage, J.J. Dubowski, Opt. Express 17 (2009) 10411–10418.
[6] D. Lepage, A. Jimenez, D. Carrier, J. Beauvais, J.J. Dubowski, Opt. Express 18 (2010) 27327–27335.
[7] S. Zhang, L. Berguiga, J. Elezgaray, T. Roland, C. Faivre-Moskalenko, F. Argoul, Surf. Sci. 601 (2007) 5445–5458.
[8] H. Raether, Surface Plasmons on Smooth and Rough Surfaces and on Gratings, Springer-Verlag, Germany, 1988. pp. 40–90.
[9] D. Christensen, D. Fowers, Biosens. Bioelectron. 11 (1996) 677–684.
[10] M.B. Kyung, J.Y. Soon, D. Kim, S.J. Kim, J. Opt. Soc. Am. A 24 (2007) 522–529.
[11] D. Lepage, A. Jimenez, D. Carrier, J.J. Dubowski, Nanoscale Res. Lett. 6 (2011) 388–395.
[12] H.G. Tompkins, E.A. Irene, Handbook of Ellipsometry, Springer-Verlag, William Andrew Inc., USA, 2005. pp. 147–246.
[13] B. Josh, C.M. Herzinger, Phys. Status Solidi C 5 (2008) 1031–1035.
[14] B. Blum, R.C. Salvarezza, A.J. Arvia, J. Vac. Sci. Technol. B 17 (1999) 2431–2438.
[15] J. Park, J.M. Kang, D.W. Kim, J.S. Choi, Thin Solid Films 518 (2010) 6232–6235.